

Delayed phosphate release can highly improve energy efficiency of muscle contraction

Jiaxiang Xu^{1#}, Jiangke Tao^{1#}, Bin Chen^{1,2*}

¹Department of Engineering Mechanics, Zhejiang University, Hangzhou, China

²Key Laboratory of Soft Machines and Smart Devices of Zhejiang Province, Hangzhou, China

These authors contributed equally.

* To whom correspondence should be addressed: chenb6@zju.edu.cn

Abstract

Although the power stroke of myosin and the release of inorganic phosphate (Pi) are pivotal in the conversion of ATP's chemical energy into mechanical work, the precise sequence of these two events remains a subject of debate. Here, we take a different path and choose to investigate how Pi-release that is not directly coupled with the power stroke affects muscle contraction. Utilizing a cross-scale mechanics model for a sarcomere unit that integrates the chemomechanical cycle of individual myosins, we find that relatively slow Pi-release can markedly improve energy efficiency during muscle contraction *in silico*. Our analysis suggests that gradual Pi-release may offer a route to finely adjust the bond strength of an attached myosin, thereby indirectly modulating the power stroke to influence muscle performance. When our model is applied to simulate muscle performance in response to rapid jumps in Pi concentrations, we observe asymmetric rates of force alteration, which corroborate previous experimental findings. Indeed, our model's predictions in the current work are largely consistent with experimental data. This work can provide important insights into the kinetics and the function of Pi-release in the regulation of forces and motions generated by myosins for cellular processes, and how to target molecular steps within the chemomechanical cycles of myosin in treating relevant pathologies.

Introduction

The captivating dance of events within the chemomechanical cycle of a myosin during muscle contraction continues to unveil its mysteries (Huxley, 1969; Lymn and Taylor, 1971; Eisenberg and Hill, 1985; Finer et al., 1994; Vale and Milligan, 2000; Woody et al., 2019; Debold, 2021; Hwang et al., 2021; Moretto et al., 2022; Marang et al., 2023). Understanding the physiological sequences of these molecular events is not only crucial to elucidating the fundamental mechanisms that govern muscle dynamics, but also significant for treating relevant pathologies (Malik et al., 2011; Woody et al., 2018; Debold, 2021; Scellini et al., 2021). Among these events, the power stroke of a myosin and its Pi-release are regarded as key steps in the transduction from ATP chemical energy to the mechanical work (Huxley, 1957; Huxley, 1969; Finer et al., 1994; Warshaw et al., 2000; Piazzesi et al., 2002; Veigel et al., 2003; Linari et al., 2015;). Since both events occur rapidly after binding to actin, it is very challenging to determine which event occurs first (Lymn and Taylor, 1971; Bagshaw and Trentham, 1974; Capitanio et al., 2012; Muretta et al., 2015). Early experiments employing photosensitive phosphate compounds revealed a noticeable time interval before any reduction in force, subsequent to Pi-release, which led to the hypothesis that the power stroke occurred immediately upon binding, followed by Pi-release (Dantzig et al., 1992). However, models representing Pi-release preceding the power stroke or the power stroke occurring prior to Pi-release were both capable of reproducing the reported relationship between force and velocity (Smith, 2014; Månsson et al., 2015; Månsson, 2019; Offer and Ranatunga, 2020).

Recent studies using high-resolution biophysical techniques measured the maximal rate of the power stroke in fast skeletal muscle myosin II at $>350/s$, while the Pi-release rate was only about $200/s$ (Trivedi et al., 2015). However, it was suggested that Pi-release may still precede the power stroke, but the released Pi relocates near ADP active sites rather than immediately returning to the solution (Llinas et al. 2015), which implied that Pi detection in the solution followed the power stroke. This proposed mechanism seems to contradict against the later finding of no significant difference in kinetics and movement rates of a wild-type myosin Va construct with increasing Pi

concentrations (Scott et al., 2021). Using cardiac muscle myosin II, it was found that the addition of 10 mM Pi to the experimental buffer did not affect the power stroke rate or size in cardiac myosin (Woody et al., 2019), which also suggested that the power stroke preceded Pi-release. Although the precise sequence of Pi-release and the power stroke remains a subject of considerable debate, it appears to be agreed that Pi-release into the solution doesn't occur instantly upon the binding of a myosin to actin.

In addition to detaching from the actin filament via the normal ATP hydrolysis cycle, it is recognized that an attached myosin can also separate through direct bond breaking (Chen and Gao, 2011). While the normal ATP hydrolysis cycle has garnered wide interest (Cooke, 1997), bond breaking of a myosin appears to have received relatively less attentions. Based on detachment rates obtained with a force spectroscopy technique of an unprecedented spatial-temporal resolution (Capitanio et al., 2012), rates of bond breaking of a myosin at different nucleotide states were systematically extracted by considering coupling between bond breaking and state transition (Dong and Chen 2016), which were found to vary strongly with nucleotide states and also forces. Among different nucleotide states, the bond formed at the AM.ADP.Pi state can be relatively weak with a very short lifetime (Pate and Cooke, 1989; Woody et al., 2019). It was also reported that bonds formed between an attached myosin and actin filaments exhibit the counter-intuitive catch-bond behavior (Guo and Guilford 2006), characterized by an increase in lifetime in response to applied forces (Dembo et al., 1988), which can provide a crucial means to stabilize attachment precisely when needed (Konstantopoulos et al., 2003; Thomas et al., 2008;).

In the present study, we diverge from the usual approach of scrutinizing the molecular-level sequence of Pi-release and the power stroke, opting instead to examine how relatively slow Pi-release that is not directly coupled with the power stroke affects muscle contraction. To this end, we implement a cross-scale mechanics model of the sarcomere unit, based on which we predict a range of muscle contraction characteristics, including force-velocity relationships, the number of “Working” motors against filament loads, and the variation of power consumption with filament loads, among others, which are found to be largely consistent with experiment. Our analytical

findings indicate that relatively slow Pi-release not directly coupled with the power stroke can significantly boost energy efficiency, when synergized with particular bond-breaking mechanisms. Our results suggest that Pi-release can serve as a regulator of the bond strength in 'Working' myosin to indirectly modulate the power stroke, thereby influencing muscle performance. Additionally, our model simulates the impact of bidirectional rapid jump in [Pi] on muscle function, revealing asymmetric rates of force alteration that resonate with empirical data (Tesi et al., 2000). We contend that this research sheds light on the critical role and function of Pi-release in the regulation of muscle contraction, enriching our understanding of this intricate biological process.

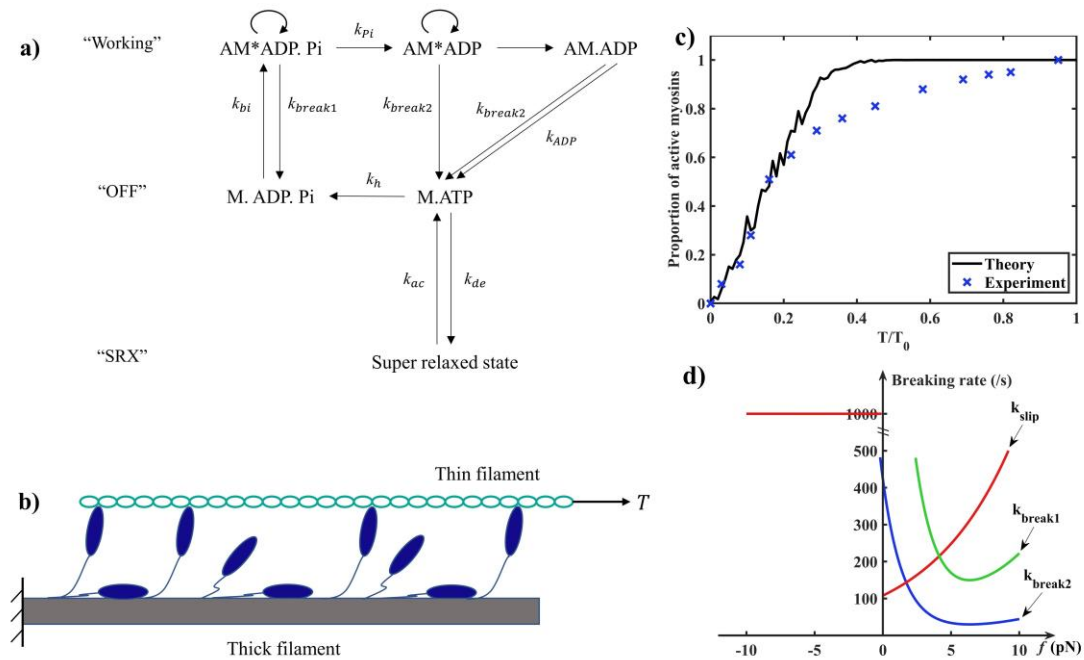


Fig. 1 a) State map of a myosin motor within a chemomechanical cycle; b) Illustration of a half sarcomere unit for skeletal muscle contraction: the thin filament (in cyan), myosin motors (in blue), and the thick filament (in grey) with a portion of motors being in the “SRX” state; c) Variation of the proportion of active motors with the developed filament load; d) Variations of bond breaking rates with force for three different bonds, including two catch bonds and one slip bonds, adopted in the analysis.

Results

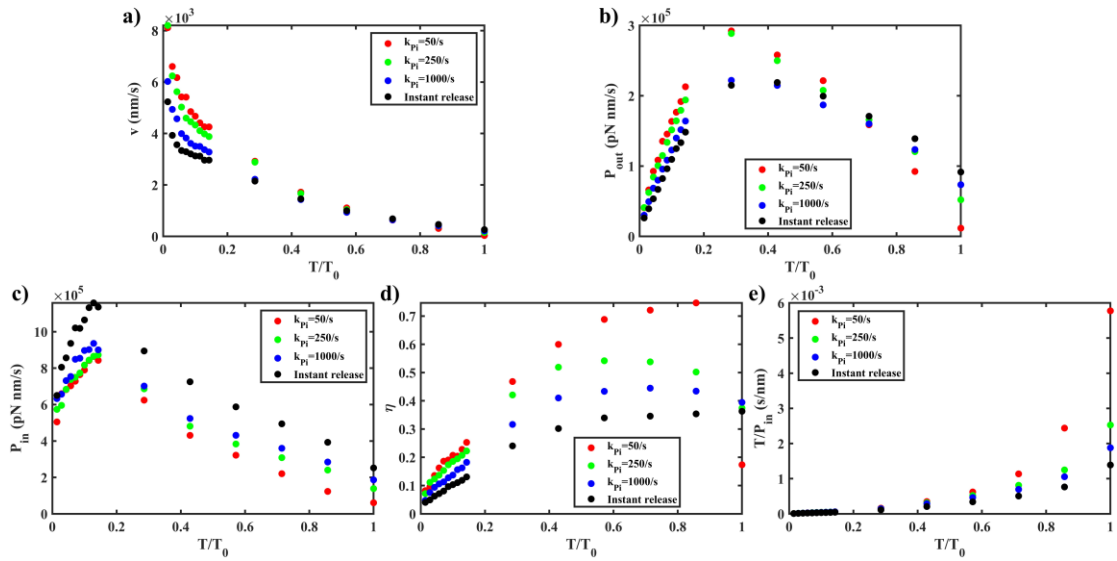


Fig. 2 Predicted features of muscle contraction at different Pi-release rates: a) The shortening velocity versus the filament load; b) The output power versus the filament load; c) Power consumption versus the filament load; d) Energy efficiency versus the filament load; e) Induced force per unit power consumption versus the filament load.

With the cross-scale mechanics model of a sarcomere unit described in Method and illustrated in Fig. 1, we investigate the effect of the Pi-release rate on features of muscle contraction, with results shown in Figs. 2-3. Note that the smaller the Pi-release rate is, the more likely a power stroke would proceed earlier than Pi-release. A special case is also considered in the simulation, where Pi-release instantly occurs upon the binding of a myosin to the actin filament, which can also be regarded with an extremely high Pi-release rate. The predicted steady-state shortening velocities versus the filament loads are plotted in Fig. 2a, where the shortening velocities generally decrease with the Pi-release rate. The difference among predictions for different Pi-release rates is prominent at low to moderate filament loads, but very small at high filament loads. The predicted isometric force only slightly increases with the Pi-release rate. We have then employed a force value very close to the predicted isometric force for the Pi-release rate of 50/s, denoted as T_0 , to scale all filament loads in Figs. 2-4.

As displayed in Fig. 3d, we observe in our simulations that a significant portion of “Working” motors detach from the thin filament through bond breaking, which generally increases as the Pi-release rate increases. In our model, with Pi being released, a “Working” motor would transit from the AM*ADP.Pi state with a relatively higher bond breaking rate to the AM*ADP state with a relatively lower bond breaking rate. If the Pi-release rate increases, this transition will occur earlier so that a “Working” motor will be less likely to detach from the thin filament through the bond breaking, which can exert dragging force against the shortening of the thin filament, especially at low to moderate filament loads with relatively large shortening velocities. This would explain why the predicted shortening velocities filament loads are generally reduced as the Pi-release rate increases in Fig. 2a.

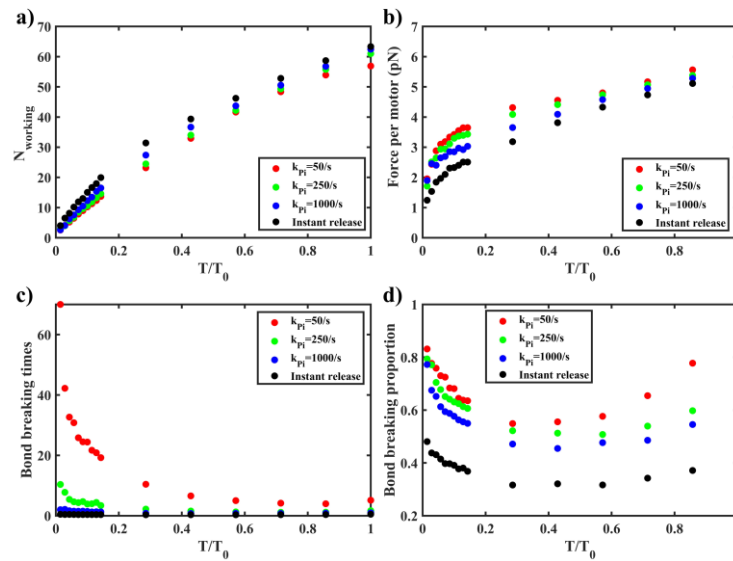


Fig. 3 Predicted features of “Working” motors at different Pi-release rates: a) Number of “Working” motors versus the filament load; b) Force per “Working” motor versus the filament load; c) Bond breaking times of a myosin with one hydrolyzed ATP versus the filament load; d) Bond breaking proportion of “Working” motors detaching from the thin filament.

Based on the simulated shortening velocity versus the filament load, we furtherly calculate the output power of the skeletal muscle during the steady-state shortening,

shown in Fig. 2b. As seen in Fig. 2b, the output power increases then decreases with the filament load. Importantly, its peak value occurs at a filament load being about 1/3 of the isometric load, in consistency with experiment (Piazzesi et al., 2007; Pertici et al., 2023). The difference among the predictions for different Pi-release rates appears to be significant and output power generally increases with the decrease of the Pi-release rate at low to moderate filament loads and the peak value of the output power is highest for the lowest Pi-release rate.

Individual myosin motors were previously found to maintain a force of ~ 6 pN and the force-velocity relationship was regarded as primarily a result of a change in the number of “Working” motors in proportion to the filament load (Piazzesi et al., 2007). We then predict the number of “Working” myosins versus the filament load, shown in Fig. 3a. In Fig. 3a, the number of “Working” motors approximately linearly increases with the filament load for different Pi-release rates, in consistency with experiment (Piazzesi et al., 2007). The predicted force per “Working” motor versus the filament load is shown in Fig. 3b, where the motor force at relatively high filament loads is regulated about 6 pN, which coincides with the stall force of a single motor in our analysis, in consistency with experiment (Piazzesi et al., 2007). However, we would like to emphasize that the motor force at low filament loads is substantially lower than 6 pN in Fig. 3b, which indeed can also be seen from previous experiments (Piazzesi et al., 2007). Small motor forces at low filament loads in our analysis are mainly due to that the relatively large shortening velocities at low filament loads would make the force on a “Working” motor relatively small. Due to small motor forces at low filament loads, the corresponding times of catch bond breaking of a myosin with one hydrolyzed ATP can be very large, as seen in Fig. 3c, which increases as the Pi-release rate decreases.

We also calculate the power consumption during the steady-state shortening, denoted as P_{in} , considering the chemical energy stored within one ATP being $p_0=50.7$ pN nm. As seen in Fig. 2c, the power consumption increases and then decreases with the filament load. Excitingly, when the Pi-release rate is higher than 250/s in our analysis, the power consumption corresponding to the maximal power output during the steady-state shortening is about 3 times of that at the isometric loading condition, in

consistency with experiment (Pertici et al., 2023). The Pi-release rate strongly affects the power consumption and increasing the Pi-release rate would generally increase the power consumption at low to moderate filament loads. These results are understandable. As the Pi-release rate gets lower, a myosin is more likely to detach through bond breaking with Pi being still in its pocket, which can then rebind to the actin filament to perform power strokes without consuming another ATP.

Based on results shown in Figs. 2b,c, we are able to calculate the energy utilization efficiency, denoted as η , during the muscle contraction, which is the ratio of the output power to the power consumption, given by η . The energy utilization efficiency during muscle contraction at different filament loads is shown in Fig. 2d. From Fig. 2d, it can be seen that the Pi-release rate strongly affects the energy utilization efficiency, and increasing the Pi-release rate would substantially decrease the energy efficiency at low to moderate filament loads. These results are understandable, since increasing the Pi-release rate would generally reduce the power consumption but increase the output power at the same time, as shown in Figs. 2b,c.

Note that the energy utilization efficiency exactly at the isometric load would be zero. In the close vicinity of the isometric load, the main function of the muscle contraction should sustain load instead to output power. Based on results shown on Fig. 2a, we then calculate the induced force per unit power consumption by dividing the filament load with the corresponding power consumption. It generally increases with the filament load, as seen in Fig. 2e. It also substantially decreases as the Pi-release rate increases in the vicinity of the isometric load, indicating a relatively low Pi-release rate would also increase the energy efficiency at high filament loads. This result is understandable. As the Pi-release rate gets lower, a myosin is more likely to detach through bond breaking with Pi being still in its pocket, which can then rebind to the actin filament to sustain load without consuming another ATP.

Discussions

In our model, a “Working” motor can either detach from actin filament through the normal ATP cycle (Lymn and Taylor, 1971) or directly break from the thin filament as

a molecular bond (Guo and Guilford, 2006; Capitanio et al. 2012; Chen and Dong 2016). Based on our predicted results shown in Figs. 3c,d, bond breaking of a “Working” myosin may occur quite often in muscle contraction. To better understand the effect of bond breaking of a “Working” myosin on muscle contraction, we turn off the catch bond breaking, denoted as “No breaking”, or change it to slip bond breaking in the analysis. In our analysis, the breaking rate of a slip bond, denoted as k_{slip} , is given by the Bell’s law (Bell 1978), $k_{slip} = k_{slip}^0 e^{\frac{f}{b}}$, which monotonically increases with the bond force when $f > 0$. To prevent dragging of attached myosins on the sliding thin filament, we have enforced $k_{slip}=1000/s$ when $f < 0$ in the analysis, as displayed in Fig. 1d. Simulation results are shown in Fig. 4. Both “No breaking” and “Slip bond” substantially decrease the shortening velocity in Fig. 4a and also the output power of the muscle at low to moderate filament loads in Fig. 4d. The maximum of output power with “No breaking” or “Slip bond” is much lower than that with catch bond breaking and occurs about 50% of the isometric load, which is inconsistency with experiment (Piazzesi et al., 2002). In Fig. 4b, the number of “Working” motors for both “No breaking” and “Slip bond” only slightly varies with the filament load so that the motor force almost linearly increases with the filament load, which is inconsistency with experiment (Piazzesi et al., 2007). Note that this result contradicts against the prediction in a previous study, where a different model of a single myosin was employed (Dong and Chen 2015). We also find that a significant portion of motors are subjected to a negative bond force at low filament loads for “No breaking”. In Fig. 4e, the power consumption almost monotonically decreases with the filament load for both “No breaking” and “Slip bond”, which is inconsistency with experiment (Smith et al., 2005). In Fig. 4f, the energy efficiency for “No breaking” or “Slip bond” at low filament loads is dramatically improved by the catch bond. These results suggest that the predictions of “No breaking” or “Slip bond” are often inconsistent with experiment and bond breaking strongly regulates features of muscle contraction. Note that, though a slip bond with very high breaking rate was reported for the AM.ADP.Pi state (Capitanio et al., 2012), this state was suggested to correspond to the weak binding state (Brenner 1991;

Geeves 1991) before producing any working stroke.

As seen from our predictions in Fig. 3, the motor force is relatively small at low to moderate filament loads. With the catch bond breaking adopted in our analysis, a “Working motor” can quickly detach upon small motor forces so that it will not drag against a shortening filament at low to moderate filament loads. With Pi being still in the nucleotide pocket due to a relatively low Pi-release rate, the detached motor can then rebind to the actin filament to perform more power strokes. In this way, the energy efficiency in muscle contraction is improved at low to moderate filament loads with the synergy of Pi-release and the bond breaking. On the other hand, the motor force at high filament loads is regulated about 6 pN, which is close to the optimal value with the longest lifetime for the catch-bond breaking so as to sustain the filament load. With Pi-release, the lifetime of the catch-bond breaking would be furtherly extended, as assumed in our model. Therefore, we suggest that particular bond breaking lifetime of a “Working” motor regulated by both force and Pi-release, such as different catch bonds adopted in our analysis, might have been selected by mother nature to improve the muscle performance.

Curiously, it was proposed that Pi-release from a “Working” myosin occurs in multiple stages, with Pi being directed through a back door and temporarily binding to at least two sites external to the active site. This mechanism was suggested to help tune the energy transduction of the actomyosin system (Moretto et al., 2022). Consistently, based on our analysis, we furtherly suggest that a gradual Pi-release may provide one route to finely tune the bond strength between a “Working” myosin and the actin filament together with the motor force so as to regulate muscle contraction. On the other hand, we have considered in the model that a detached motor, containing both ADP and Pi within its nucleotide pocket, can reattach to the actin filament to subsequently execute a power stroke, whereas a motor with only ADP being in its nucleotide pocket immediately releases the ADP. Such a treatment implies that Pi is also assumed to play a role related to the control of the energy release of a detached myosin in the model.

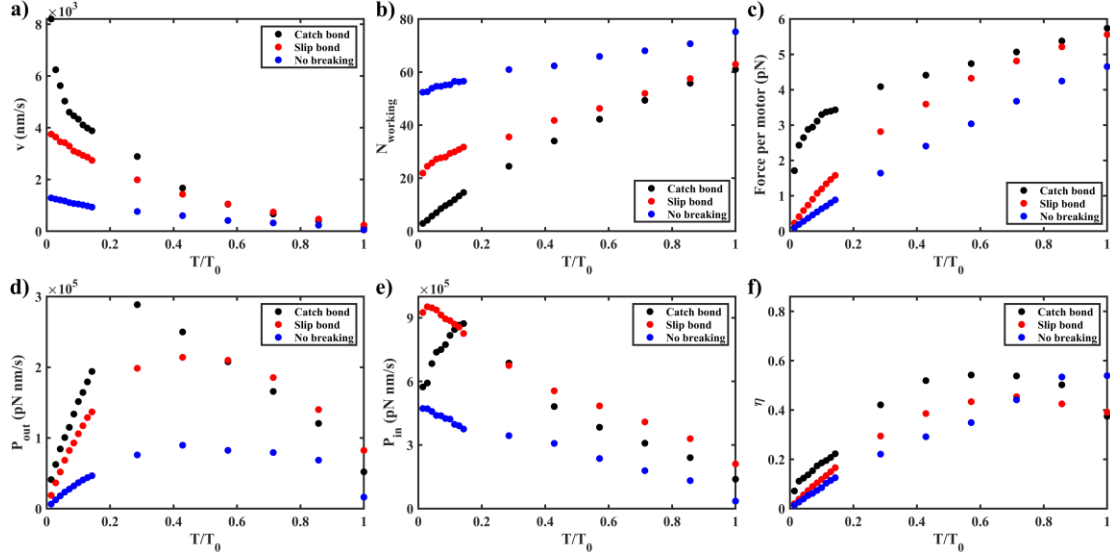


Fig. 4 Predicted features of muscle contraction with slip bond breaking or no breaking compared to those with catch bond breaking: **a)** The shortening velocity versus the filament load; **b)** Number of “Working” motors versus the filament load; **c)** Force per “Working” motor versus the filament load; **d)** The output power versus the filament load; **e)** Power consumption versus the filament load; **f)** Energy efficiency versus the filament load.

As also reported in the literature, the rate constant of tension decrease with a rapid increase in $[Pi]$ can be surprisingly different from that of tension increase with a rapid decrease in $[Pi]$ within muscles (Tesi et al., 2000; Stehle and Tesi, 2017). To investigate effects of the rapid jump in $[Pi]$ on the muscle contraction, we furtherly consider in our model that, a Pi can rebind to a “Working” myosin at the AM.ADP state so that the myosin would transit back to the AM.ADP.Pi state, which was thought to potentially enhance the energy utilization efficiency of muscles (Robert-Paganin et al., 2020). The rebinding rate of Pi to the AM.ADP state, denoted as k_{bind} , was suggested to be affected by force (Marang et al. 2023), as well as by $[Pi]$. For simplification, k_{bind} is only affected by $[Pi]$ in our consideration, given by the Michealis–Menten equation (Xie, 2013), $k_{bind} = k_{max}[Pi]/(c_M + [Pi])$, where k_{max} is the maximal rebinding rate of Pi and c_M is the Michaelis–Menten constant. In our simulations, the rapid jump

in [Pi] is superposed to the isometric loading condition. The simulated tension time courses are displayed in Fig. 5. In Fig. 5a, an isometric filament load is generated at 50 mMol [Pi], followed by a rapid decrease in [Pi] to 5 mMol. In Fig. 5b, an isometric filament load is generated at 5 μ Mol of [Pi], followed by a rapid increase in [Pi] to 5 mMol. A transient release and then stretch at the same [Pi] of 5 mMol superposed to the isometric loading condition is also simulated, with results shown in Fig. 5c. With results shown in Figs. 5d-f, we extract the rate constant of tension change due to the transient release and then stretch, denoted as k_{TR} , that following the rapid increase in [Pi], denoted as $k_{Pi(+)}$, and that following the rapid decrease in [Pi], denoted as $k_{Pi(-)}$, respectively. The exacted rates are $k_{TR} = 90.0/s$, $k_{Pi(+)} = 177.7/s$, and $k_{Pi(-)} = 88.2/s$, respectively, where $k_{Pi(-)}$ is close to k_{TR} at same [Pi], while $k_{Pi(+)}$ is much higher than k_{TR} at same [Pi], which agrees with previous experiments (Tesi et al., 2000).

The asymmetric kinetic rates obtained in bi-directional rapid jumps of [Pi] in our simulations are closely related to varied bond breaking rates from different states of a “Working” myosin. In our simulations, the bond breaking rate from the AM.ADP.Pi state is set to be five times of that from AM.ADP state. At high [Pi] conditions, more motors would be at the AM*ADP.Pi state with a larger bond breaking rate, leading to a decrease in the total number of “Working” motors and a subsequent reduction in the isometric force, as indicated in Figs. 5b. With a rapid increase in [Pi], a portion of myosins will transit directly from the AM.ADP state back to the AM.ADP.Pi state and then detach from the actin filament with bond breaking without going through the whole chemomechanical cycle, leading to a larger $k_{Pi(-)}$ than k_{TR} . Such a scenario appears to be consistent with the suggested sarcomere “give” in the literature (Flitney and Hirst, 1978). With a rapid decrease in [Pi], a portion of myosins would transit from the AM.ADP.Pi state to the AM.ADP state. Meanwhile, with a larger isometric load resulted from the decreased [Pi], a portion of myosins are needed to recruit from either “OFF” state or “SRX” state, which would more or less go through the whole chemomechanical cycle of myosins. This would lead to a comparable $k_{Pi(+)}$ with k_{TR}

in our analysis. Such a scenario appears to be consistent with the previous suggestion that the force rise upon the decrease in $[Pi]$ more closely reflects overall sarcomere cross-bridge kinetics (Tesi et al., 2000).

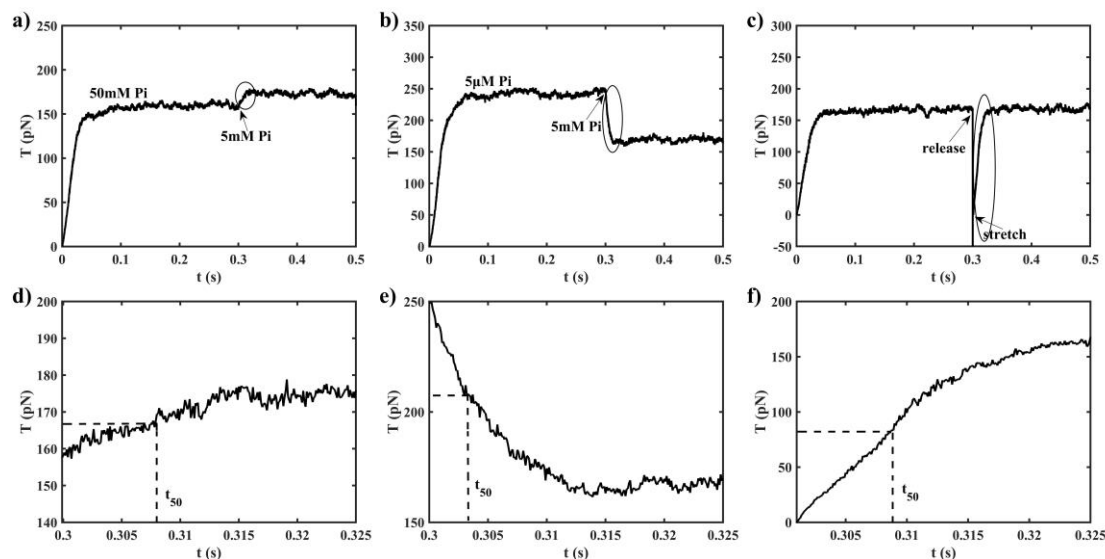


Fig. 5 Predicted time course of the change in the isometric force due to rapid jump in $[Pi]$ (a, b) or that due to a transient release and then stretch (c): a) Force response of a sarcomere unit activated in 50 mM $[Pi]$ solution and then subjected to a $[Pi]$ jump to 5 mM; b) Force response of a sarcomere unit activated in 5 μ M $[Pi]$ and then subjected to a $[Pi]$ jump to 5 mM; c) Force response of a sarcomere unit activated in 5 mM $[Pi]$ solution and then subjected to a transient release and then stretch. Zoomed in regions circled out in (a-c) are re-plotted in (d-e), respectively.

In above analysis, we have assumed that rate coefficients of multiple possible rebinding of a detached myosin with Pi still being in its nucleotide pocket are the same. We also consider the possibly that this rebinding rate is affected, for example, by the accumulated swing distance of the power stroke. In our consideration, this rebinding rate is reduced 50% when the accumulated swing distance is above 3 nm. Our predicted results are shown in Fig. 6. When compared with no effect on the rebinding rate from the accumulated swing distance, the shortening velocity will now get lower. The impact on the number of “Working” motor, motor force, or the power consumption is relatively

small. The energy efficiency will get lower, making our prediction even closer to the reported energy efficiency in the literature (Smith et al., 2005).

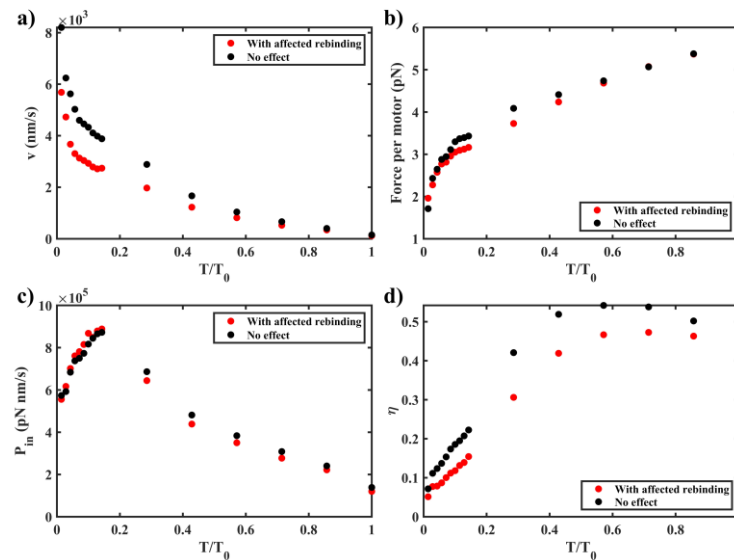


Fig. 6 Predicted features of muscle contraction with or without affected rebinding rates of a detached myosin with Pi being in its nucleotide pocket by the accumulated swing distance of its lever arm: a) Shortening velocity versus the filament load; b) Force per motor versus the filament load; c) Power consumption versus the filament load; d) Energy efficiency versus the filament load.

Finally, we would like to point out that, in our cross-scale mechanics model, the lever arm of a “Working” myosin can swing multiple times within the power stroke, and each swing can be arrested at the stall force, which determines the swing distance (Chen 2013). Such a treatment in the model (Chen 2013) was shown to capture main features of force-stretch curves of a “working” myosin extracted from the muscle transient test (Piazzesi and Lombardi 1995). Interestingly, when we assume that there exist multiple sub-states within the power stroke and the transition between neighboring sub-states is similarly force-regulated, which is associated with a small and fixed swing distance of the lever arm, for example, 1nm, we can also make reasonably good predictions of force-stretch curves of a “Working” myosin. This suggests that each

swing of lever arm in our model prediction may be physically related to the transition among sub-states potentially existing within the power stroke (Huxley and Simmons 1971).

Conclusion

With a cross-scale mechanics model of a sarcomere unit, we make predictions of various features of muscle contraction *in silico*, which are largely consistent with experiment. Based on our analysis, we reveal that relatively slow Pi-release can be synergetic with bond breaking of a “Working” myosin, leading to the improved energy efficiency in muscle contraction. We furtherly suggest that a gradual Pi-release might help finely tune the bond strength between a “Working” motor and actin to indirectly modulate the power stroke so as to regulate overall performance of muscle contraction. We believe that this work can provide important insights into the kinetics and the function of Pi-release in the regulation of forces and motions generated by myosins for cellular processes they orchestrate, and how to target molecular steps within the chemomechanical cycles of myosin in treating relevant pathologies.

Method

Mainly based on the classical Lymn-Taylor scheme (Lymn and Taylor, 1971), a state map within the chemomechanical cycle of a single myosin is constructed. As illustrated in Fig. 1a, six states in total are assigned, including SRX, M.ATP, M.ADP.Pi, AM*ADP.Pi, AM*ADP, and AM.ADP. Among them, M.ATP and M.ADP.Pi are grouped together as the “Off” state and AM*ADP.Pi, AM*ADP, and AM.ADP are grouped together as the “Working” state, respectively.

At SRX state, so called the super relaxed state (Linari et al., 2015), a myosin is deactivated and can't bind to the actin filament. The transition rate between the SRX state and the M.ATP state would be regulated by the filament load due to the mechanosensing of the thick filament (Linari et al., 2015). A myosin transits from the M.ATP state to the M.ADP.Pi state when the hydrolyzation of ATP takes place. When a

myosin is at the M.ADP.Pi state, it can bind to the thin filament through the Brownian motion.

When a myosin binds to the thin filament, the myosin will be at the AM*ADP.Pi state or the AM*ADP state with Pi-release. While it is controversial whether Pi-release occurs before or after the power stroke in the literature (Muretta et al., 2015; Woody et al., 2019; Governali et al., 2020; Stehle, 2017; Llinas et al., 2015; Malnasi-Csizmadia and Kovacs, 2010; Månsson et al., 2015; Stehle and Tesi, 2017; Scott et al., 2021; Smith, 2014; Homsher, 2017), we have assumed that Pi-release from the AM*ADP.Pi state is not directly coupled with the power stroke in the current work (Muretta et al., 2015; Trivedi et al., 2015). At the AM*ADP.Pi state or the AM*ADP state, the lever arm of a myosin can swing forward multiple times within the power stroke with both the rate and the distance of each swing being regulated by force (Chen, 2013) and the swing would be temporarily arrested beyond a stall force, denoted as f_a , which was found to increase with the temperature (Dong and Chen, 2016). When the accumulated swing distance of a myosin due to one hydrolyzed ATP reaches the maximum (Chen, 2013), denoted as L_s , which was found to decrease with the temperature (Dong and Chen, 2016), the lever arm would not be able to swing any more. Note that the backward swing of the lever arm is neglected in the current model, which can be low for fast skeletal myosin but essential for cardiac myosin (Hwang et al., 2021).

When the accumulated swing distance of the lever arm due to one hydrolyzed ATP reaches the maximum, the myosin will release the ADP and capture an ATP to quickly detach from the actin filament. Alternatively, a motor can detach from the actin filament at any “Working” state directly through bond breaking (Brenner, 1991; Guo and Guilford, 2006; Chen and Gao, 2011; Capitanio et al., 2012; Dong and Chen, 2016). If the motor detaches through bond breaking at the AM*ADP.Pi state, it can rebind to the actin filament through the Brownian motion with ADP and Pi being still in its pocket (Brenner, 1991). The total accumulated swing distance of the lever arm during multiple possible attachments due to one hydrolyzed ATP is assumed to be less than L_s , beyond which the lever arm will not swing anymore. If a myosin detaches through bond breaking at the AM*ADP state or the AM.ADP state, it will quickly release the ADP

and then catch an ATP to reach the M.ATP state.

Non-negligible transition rates among different states of a myosin considered in the model are displayed in Fig. 1a. The transition rate from the SRX state to the M.ATP state of a myosin is denoted as k_{ac} . With the Bell's formula (Bell, 1978), $k_{ac} = k_{01} \exp\left(\frac{T}{T_{01}}\right)$, where k_{01} is the corresponding transition rate without force and T_{01} is a force scale. The backward transition rate from the M.ATP state to the SRX state of a myosin is denoted as k_{de} . With the Bell's formula (Bell, 1978), $k_{de} = k_{10} \exp\left(-\frac{T}{T_{01}}\right)$, where k_{10} is the corresponding transition rate without force. As seen in Fig. 1c, with k_{ac} and k_{de} being regulated by the filament load, the proportion of activated myosins that are at both OFF and Working states in our analysis increases with the filament load until saturates in the vicinity of the isometric filament load, close to experiment (Linari et al., 2015).

The transition rate from the M.ATP state to the M.ADP.Pi state, denoted as k_h , is set to be a constant. A “Working” myosin is modeled as a passive linear spring, which is in series with a rigid lever arm that can actively swing (Chen and Gao, 2011). The myosin binding rate from the M.ADP.Pi state to the AM*ADP.Pi state is given by $k_{bi} = \sqrt{\frac{\beta}{\pi}} 2\xi \exp(-\beta U^2) / [1 + \operatorname{erf}(0.3\sqrt{\beta})]$ (Chen and Gao, 2011), where $\beta = s_m l_a^2 / (2k_B T)$, with s_m being the spring constant of the myosin, k_B the Boltzmann constant, T the absolute temperature, l_a the spacing between neighboring binding sites on the thin filament, $U = u/l_a$, with u being the separation between the myosin and its binding site on the thin filament, and ξ is a rate constant.

The Pi-release rate from the AM*ADP.Pi state, denoted as k_{pi} , is set to be a constant. The relationship between motor force at the AM*ADP.Pi state or at the AM*ADP state, denoted as f , and motor stretch, denoted as x , is given by $f = s_m x$, with $x = u + d$, where d is the accumulated swing distance of the lever arm. d is initially set to be zero upon the first attachment of a myosin with a hydrolyzed ATP to the thin filament.

The bond lifetime formed between myosin and actin varies with the state of a “Working” myosin (Guo and Gilford 2006; Capitanio et al., 2012). The bond formed at

the AM.ADP state was suggested to be a catch bond (Guo and Gilford 2006; Dong and Chen 2016), with its lifetime counterintuitively increasing and finally decreasing with force. Importantly, the maximum bond lifetime was found to be near the stall force of a myosin (Guo and Gilford 2006). In the current work, by default, we assume that the bond formed between myosin and actin at different “Working” states is a catch bond with the bond breaking rate, denoted as k_{catch} , being given by $k_{catch} = \vartheta \left(50 \exp\left(-\frac{f}{1.5}\right) + \exp\left(\frac{f}{6}\right) \right)$ (Chen and Gao, 2011), where f is of a unit of pN and ϑ is a rate constant. Note that the bond formed at the AM*ADP.Pi state can be relatively weak (Pate and Cooke, 1989; Woody et al., 2019). As illustrated in Fig. 1d, the catch-bond breaking rate is set to be lower at the AM*ADP state or at the AM.ADP state, denoted as k_{break2} , than that at the AM*ADP.Pi state, denoted as k_{break1} , which is realized by assigning a smaller ϑ at the AM*ADP state or at the AM.ADP state, denoted as ϑ_2 , than that at the AM*ADP.Pi state, denoted as ϑ_1 . The lumped kinetic rate from the AM.ADP state to the M.ATP state through the normal ATP cycle is set to be a constant, denoted as k_{ADP} .

The swing rate of a lever arm within the power stroke depends on the motor force. When the motor force $f < f_a$, the motor mainly swing forward at a rate given by $k_f = k_{f0} \exp[(f_a - f)/f_a]$ (Chen, 2013), where k_{f0} is the forward swing rate at $f = f_a$. When the motor force $f > f_a$, the swing of the motor is assumed to be arrested. The distance of each swing within the power stroke is given by $\Delta x = (f_a - f)/s_m$.

Due to symmetry, only half of a sarcomere as the structural unit of the skeletal muscle is considered in developing the cross-scale mechanics model for the muscle contraction (Chen and Gao, 2011). As illustrated in Fig. 1b, the model consists of the thin filament, the thick filament and multiple myosin motors uniformly distributed along the thick filament. The total number of myosins in the model is denoted as N_m and the separation between neighboring myosins is denoted as l_m . The thick filament is fixed on its left end while the thin filament is subjected to a filament load, denoted as T , on its right end. In the model, the thin filament in the sarcomere is modeled as an elastic rod with axial rigidity, EA_{thin} , and the thick filament is also modeled as an

elastic rod with axial rigidity, EA_{thick} .

The numerical method employed in our work is a coupled Monte Carlo method and Finite-element method (Chen and Gao, 2011; Dong and Chen, 2015). Initially, most myosin motors are set to be at the SRX state, and only a few constitutively on myosin motors, which is set to be 5, are at the AM*ADP.Pi state (Linari et al., 2015). In the Finite-element method, the thin filament is discretized into one-dimensional two-node rod elements, each motor corresponds to a linear spring element, and the thick filament elasticity is also represented with one-dimensional two-node rod elements. A motor within the sarcomere may change its state with time. Thus, the stiffness matrix of the whole structure and the nodal force vector are updated at each time step in the simulation. The displacement for each node is subsequently solved, and motor forces are obtained. The rates of all possible stochastic events are then calculated, based on which the time needed for the i th random event to take place, τ_i , is obtained. The time needed for the next event to occur, Δt , would be the smallest among τ_i . At the end of each time step, the system is updated, and the simulation proceeds to the next step. The program used for the analysis is self-coded and default values of parameters for the analysis are listed in Table 1.

Table 1 Default values of parameters used in the simulation

| Parameter | Value | Parameter | Value |
|---------------------|---------------------------------------|--------------------|--------------------------------------|
| s_m | 3 pN/nm (Piazzesi et al., 2007) | N_m | 76 (Marcucci and Reggiani, 2016) |
| EA_{thick} | 45.8 nN | EA_{thin} | 22.7 nN |
| l_m | 14.3 nm (Marcucci and Reggiani, 2016) | l_a | 5.5 nm (Marcucci and Reggiani, 2016) |
| ϑ_2 | 8.3 /s (Chen and Gao, 2011) | ϑ_1 | 41.5 /s |
| ξ | 400 /s | T_{01} | 40 pN |
| f_a | 6 pN (Piazzesi et al., 2007) | L_s | 6 nm (Piazzesi et al., 2007) |
| k_{01} | 1000 /s | k_{10} | 200 /s |

| | | | |
|-----------|-------------------------------|-----------|--------------------------------------|
| k_{ADP} | 1000 /s (Dong and Chen, 2015) | k_h | 1440 /s |
| k_{Pi} | 250 /s (Trivedi et al., 2015) | k_{f0} | 1700 /s (Dong and Chen, 2016) |
| c_M | 1900 μmol | k_{max} | 1000 /s |
| $k_B T$ | 4.14×10^{-21} J | p_0 | 50.7 pN.nm (Bergman et al., 2010) |

Acknowledgements

This work was supported by the National Natural Science Foundation of China (Grant No.: 12372318) and Zhejiang Provincial Natural Science Foundation of China (Grant No.: LZ23A020004).

Author contributions

B.C. designed research, J.X., J.T., and B.C. performed research, J.X. and J.T. analyzed data, J.X., J.T., and B.C. wrote the manuscript.

Competing Interest Statement

The authors declare no competing interests.

References

- Bagshaw CR, Trentham DR. 1974. The characterization of myosin-product complexes and of product-release steps during the magnesium ion-dependent adenosine triphosphatase reaction. *The Biochemical Journal* 141: 331-349.
- Bell GI. 1978. Models for the specific adhesion of cells to cells. *Science* 200: 618-627.
- Bergman C, Kashiwaya Y, Veech RL. 2010. The effect of pH and free Mg²⁺ on ATP linked enzymes and the calculation of Gibbs free energy of ATP hydrolysis. *The Journal of Physical Chemistry. B* 114:16137-16146.
- Brenner B. 1991. Rapid dissociation and reassociation of actomyosin cross-bridges during force generation: a newly observed facet of cross-bridge action in muscle. *Proceedings of the National Academy of Sciences of the United States of America* 88: 10490-10494.
- Capitanio M, Canepari M, Maffei M, Beneventi D, Monico C, Vanzi F, Bottinelli R, Pavone FS. 2012. Ultrafast force-clamp spectroscopy of single molecules reveals load dependence of myosin working stroke. *Nature Methods* 9: 1013-1019.
- Chen B. 2013. Self-Regulation of Motor Force Through Chemomechanical Coupling in Skeletal Muscle Contraction. *Journal of Applied Mechanics* 80: 051013.
- Chen B, Gao H. 2011. Motor force homeostasis in skeletal muscle contraction. *Biophysical Journal* 101: 396-403.
- Cooke R. 1997. Actomyosin interaction in striated muscle. *Physiological Reviews* 77: 671-697.
- Dantzig JA, Goldman YE, Millar NC, Laktis J, Homsher E. 1992. Reversal of the cross-bridge force-generating transition by photogeneration of phosphate in rabbit psoas muscle fibres. *The Journal of Physiology* 451: 247-278.
- Debold EP. 2021. Recent insights into the relative timing of myosin's powerstroke and release of phosphate. *Cytoskeleton (Hoboken)* 78: 448-458.
- Dembo M, Torney DC, Saxman K, Hammer D. 1988. The reaction-limited kinetics of membrane-to-surface adhesion and detachment. *Proceedings of the Royal Society of London. Series B, Biological sciences* 234: 55-83.
- Dong CL, Chen B. 2015. Catch-slip bonds can be dispensable for motor force regulation during skeletal muscle contraction. *Physical review. E, Statistical, nonlinear, and soft matter physics* 92: 012723.
- Dong CL, Chen B. 2016. Coupling of Bond Breaking With State Transition Leads to High Apparent Detachment Rates of a Single Myosin. *Journal of Applied Mechanics* 83: 051011.
- Eisenberg E, Hill TL. 1985. Muscle contraction and free energy transduction in biological systems. *Science* 227: 999-1006.
- Finer JT, Simmons RM, Spudich JA. 1994. Single myosin molecule mechanics:

piconewton forces and nanometre steps. *Nature* 368: 113-119.

Flitney FW, Hirst DG. 1978. Cross-bridge detachment and sarcomere 'give' during stretch of active frog's muscle. *The Journal of physiology* 276: 449–465.

Geeves MA. 1991. The dynamics of actin and myosin association and the crossbridge model of muscle contraction. *Biophysical Journal* 274: 1-14.

Governali S, Caremani M, Gallart C, Pertici I, Stienen G, Piazzesi G, Ottenheijm C, Lombardi V, Linari M. 2020. Orthophosphate increases the efficiency of slow muscle-myosin isoform in the presence of omecantiv mecarbil. *Nature Communications* 11: 3405.

Guo B, Guilford WH. 2006. Mechanics of actomyosin bonds in different nucleotide states are tuned to muscle contraction. *Proceedings of the National Academy of Sciences of the United States of America* 103: 9844-9849.

Homsher E. 2017. A new and improved view of force production. *Biophysical Journal* 112: 205-206.

Huxley AF. 1957. Muscle structure and theories of contraction. *Progress in Biophysics and Biophysical Chemistry* 7: 255-318.

Huxley HE. 1969. The Mechanism of Muscular Contraction. *Science* 164: 1356-1366.

Huxley AF, Simmons RM. 1971. Proposed mechanism of force generation in striated muscle. *Nature* 233: 533-538.

Hwang Y, Washio T, Hisada T, Higuchi H, Kaya M. 2021. A reverse stroke characterizes the force generation of cardiac myofilaments, leading to an understanding of heart function. *Proceedings of the National Academy of Sciences of the United States of America* 118: e2011659118.

Konstantopoulos K, Hanley WD, Wirtz D. 2003. Receptor–ligand binding: 'catch' bonds finally caught. *Current Biology* : CB 13: R611-R613.

Linari M, Brunello E, Reconditi M, Fusi L, Caremani M, Narayanan T, Piazzesi G, Lombardi V, Irving M. 2015. Force generation by skeletal muscle is controlled by mechanosensing in myosin filaments. *Nature* 528: 276- 279.

Llinas P, Isabet T, Song L, Ropars V, Zong B, Benisty H, Sirigu S, Morris C, Kikuti C, Safer D, Sweeney HL, Houdusse A. 2015. How actin initiates the motor activity of Myosin. *Developmental cell* 33: 401-412.

Lynn RW, Taylor EW. 1971. Mechanism of adenosine triphosphate hydrolysis by actomyosin. *BioChemistry* 10: 4617-4624.

Malik FI, Hartman JJ, Elias KA, Morgan BP, Rodriguez H, Brejc K, Anderson RL, Sueoka SH, Lee KH, Finer JT, Sakowicz R, Baliga R, Cox DR, Garard M, Godinez G, Kawas R, Kraynack E, Lenzi D, Lu PP, Muci A, Niu C, Qian X, Pierce DW, Pokrovskii M, Suehiro I, Sylvester S, Tochimoto T, Valdez C, Wang W, Katori T, Kass DA, Shen YT, Vatner SF, Morgans DJ. 2011. Cardiac myosin activation: a potential therapeutic approach for systolic heart failure. *Science* 331: 1439-1443.

Malnasi-Csizmadia A, Kovacs M. 2010. Emerging complex pathways of the actomyosin powerstroke. *Trends in Biochemical Sciences* 35: 684-690.

Månsson A, Rassier D, Tsiavaliaris G. 2015. Poorly understood aspects of striated muscle contraction. *BioMed Research International* 2015: 245154..

Månsson A. 2019. Comparing models with one versus multiple myosin-binding sites per actin target zone: The power of simplicity. *The Journal of General Physiology* 151: 578-592.

Marang C, Scott B, Chambers J, Gunther LK, Yengo CM, Debold EP. 2023. A mutation in switch I alters the load-dependent kinetics of myosin Va. *Nature Communications* 14: 3137.

Marcucci L, Reggiani C. 2016. Mechanosensing in Myosin Filament Solves a 60 Years Old Conflict in Skeletal Muscle Modeling between High Power Output and Slow Rise in Tension. *Frontiers in physiology* 7: 427.

Moretto L, Ušaj M, Matusovsky O, Rassier DE, Friedman R, Månsson A. 2022. Multistep orthophosphate release tunes actomyosin energy transduction. *Nature Communications* 13: 4575.

Muretta JM, Rohde JA, Johnsrud DO, Cornea S, Thomas DD. 2015. Direct real-time detection of the structural and biochemical events in the myosin power stroke. *Proceedings of the National Academy of Sciences of the United States of America* 112: 14272-14277.

Offer G, Ranatunga KW. 2020. The Location and Rate of the Phosphate Release Step in the Muscle Cross-Bridge Cycle. *Biophysical Journal* 119: 1501-1512.

Pate E, Cooke R. 1989. A model of crossbridge action: the effects of ATP, ADP and Pi. *Journal of Muscle Research and Cell Motility* 10: 181-196.

Pertici I, Bongini L, Caremani M, Reconditi M, Linari M, Piazzesi G, Lombardi V, Bianco P. 2023. Matching mechanics and energetics of muscle contraction suggests unconventional chemomechanical coupling during the actin-myosin interaction. *International Journal of Molecular Sciences* 24: 12324.

Piazzesi G, Lombardi V. 1995. A Cross-Bridge Model That is Able to Explain Mechanical and Energetic Properties of Shortening Muscle. *Biophysical Journal* 68: 1966-1979.

Piazzesi G, Lucii L, Lombardi V. 2002. The size and the speed of the working stroke of muscle myosin and its dependence on the force. *The Journal of Physiology* 545: 145-151.

Piazzesi G, Reconditi M, Linari M, Lucii L, Sun Y-B, Narayanan T, Boesecke P, Lombardi V, Irving M. 2002. Mechanism of force generation by myosin heads in skeletal muscle. *Nature* 415: 659-662.

Piazzesi G, Reconditi M, Linari M, Lucii L, Bianco P, Brunello E, Decostre V, Stewart A, Gore DB, Irving TC, Irving M, Lombardi V. 2007. Skeletal muscle performance

determined by modulation of number of myosin motors rather than motor force or stroke size. *Cell* 131: 784-95.

Robert-Paganin J, Pylypenko O, Kikuti C, Sweeney HL, Houdusse A. 2020. Force generation by myosin motors: a structural perspective. *Chemical Reviews* 120: 5-35.

Scellini B, Piroddi N, Dente M, Vitale G, Pioner JM, Coppini R, Ferrantini C, Poggesi C, Tesi C. 2021. Mavacamten has a differential impact on force generation in myofibrils from rabbit psoas and human cardiac muscle. *The Journal of General Physiology* 153: e202012789.

Scott B, Marang C, Woodward M, Debold EP. 2021. Myosin's powerstroke occurs prior to the release of phosphate from the active site. *Cytoskeleton* 78: 185-198.

Smith DA. 2014. A new mechanokinetic model for muscle contraction, where force and movement are triggered by phosphate release. *Journal of Muscle Research and Cell Motility* 35: 295-306.

Smith NP, Barclay CJ, Loiselle DS. 2005. The efficiency of muscle contraction. *Progress in Biophysics and Molecular Biology* 88: 1-58.

Stehle R. 2017. Force responses and sarcomere dynamics of cardiac myofibrils induced by rapid changes in [Pi]. *Biophysical Journal* 112: 356-367.

Stehle R, Tesi C. 2017. Kinetic coupling of phosphate release, force generation and rate-limiting steps in the cross-bridge cycle. *Journal of Muscle Research and Cell Motility* 38: 275-289.

Tesi C, Colomo F, Nencini S, Piroddi N, Poggesi C. 2000. The effect of inorganic phosphate on force generation in single myofibrils from rabbit skeletal muscle. *Biophysical Journal* 78: 3081-3092.

Thomas WE, Vogel V, Sokurenko E. 2008. Biophysics of catch bonds. *Annual Review of Biophysics* 37: 399-416.

Trivedi DV, Muretta JM, Swenson AM, Davis JP, Thomas DD, Yengo CM. 2015. Direct measurements of the coordination of lever arm swing and the catalytic cycle in myosin V. *Proceedings of the National Academy of Sciences of the United States of America* 112: 14593-14598.

Vale RD, Milligan RA. 2000. The way things move: looking under the hood of molecular motor proteins. *Science* 288: 88-95.

Veigel C, Molloy JE, Schmitz S, Kendrick-Jones J. 2003. Load-dependent kinetics of force production by smooth muscle myosin measured with optical tweezers. *Nature Cell Biology* 5: 980-986.

Warshaw DM, Guilford WH, Freyzo Y, Kremmentsova E, Palmiter KA, Tyska MJ, Baker JE, Trybus KM. 2000. The light chain binding domain of expressed smooth muscle heavy meromyosin acts as a mechanical lever. *Journal of Biological Chemistry* 275: 37167-72.

Woody MS, Greenberg MJ, Barua B, Winkelmann DA, Goldman YE, Ostap EM. 2018.

Positive cardiac inotrope omecantiv mecarbil activates muscle despite suppressing the myosin working stroke. *Nature Communications* 9: 3838.

Woody MS, Winkelmann DA, Capitanio M, Ostap EM, Goldman YE. 2019. Single molecule mechanics resolves the earliest events in force generation by cardiac myosin. *eLife* 8: e49266.

Xie XS. 2013. Biochemistry. Enzyme kinetics, past and present. *Science* 342: 1457-1459.